6.0 CHARACTERIZATION OF PARTICLES BY AEM

Transmission electron microscopy (TEM), coupled with energy dispersive spectroscopy (EDS), has been shown to be an effective, powerful tool for examining geochemical question on the individual particle scale. When used together in a quantitative sense, the term analytical electron microscopy (AEM) is often used. In particular, AEM is well suited to provide information on the size, morphology, crytallinity, and elemental composition of single particles as well as on their physical and spatial associations (Leppard *et. al.*, 1988; Buffle *et. al.*, 1989). Some recent studies have used AEM to examine mineral associations in aquifers (Swartz *et. al.*, 1997), heavy metal sulfide precipitation in soils (Barnett *et. al.*, 1997), chemical speciation of metals in lakes (Lienemann *et. al.*, 1997; Perret *et. al.*, 2000; Taillefert *et. al.*, 2000), and immobilization of dissolved metals onto minerals and biomass (Patterson *et. al.*, 1997; Arey *et. al.*, 1999; Figueira *et. al.*, 1999) as well as weathering and diagenetic reactions in lake sediments (Banfield *et. al.*, 1991b; Banfield *et. al.*, 1991a). The real power of the technique arises from the ability to make measurements directly, *i.e.* by making direct observations of the particles themselves. This eliminates the averaging over many thousands of particles that may occur when looking at bulk properties of the sediments, although a large number of samples must be examined for the results to be statistically significant. Thus many of the insights that can be realized through AEM can be missed when making inferences from bulk chemical data. Thus, by combining AEM with other analytical techniques, a more developed chemical picture can be developed of the sedimentary environment.

Electron microscopy of the sediments of Lake DePue reveals the existence of several different colloid classes present in nearly all core samples. These classes can be identified through a combination of their size, shape, electron-opacity, and elemental composition as determined by STEM-EDS. The principal constituents were bacteria, small algae, organic fibrils and matrices, clay minerals, iron hydroxides, iron-zinc phosphates, biogenic silica and diatoms, and sulfidic minerals. Carbonates, defined as particles containing primarily Mg and Ca exclusively, although found in small amounts at all collection sites, were found to be a minor component among the other major particles observed. X-ray EDS analyses showed that zinc was most prevalent on particles close to the effluent source. The details of these zinc-containing phases are discussed below.

6.1 CHARACTERIZATION OF ZINC BEARING PARTICLES

Distinct trends of zinc associations on colloidal particles can be observed between the various collection sites. Figures 6.1a and 6.1b show the electron micrographs and Figures 6.2a and 6.2b present their associated EDS spectra of particles collected from the site C_1. This site is characterized by a low volume, oxic, effluent stream transporting up to 300 μM Zn over sediments that contain Zn concentrations ranging from 3% to nearly 30% by dry weight. Due to the high absolute concentration of zinc in these sediments, many of the particles from this site contain appreciable amounts of zinc. Figure 6.1a shows typical zinc-rich particles that range in size from 120 to 550 nm, have regular

shape, and have uniform electron density. A typical EDS spectrum for these particles, shown in Figure 6.2a, demonstrates that they are rich in iron, zinc, and phosphorus. This morphology is the most common of the zinc bearing colloids, which often appear to be strongly associated with and entrained into biological structures. This is evidenced in Figure 6.1b where the particles are intimately associated with an algal cell, whose organic-rich outer surface may be acting as a template or nucleation site for particle formation. The zinc in these particles must be co-precipitated or co-entrained, as such high concentrations of zinc are not likely to be present solely as a result of surface adsorption phenomena. Additionally, the EDS would not detect zinc that was merely present as surface sorbed species, as net concentrations of over a few percent are required. Other zinc containing particles at this location include iron-zinc oxyhydroxides, and to a lesser degree, particles in which zinc is sorbed onto iron-rich clay minerals.

Water column particulates from the C_2 collection site were also examined. Particles examined from this locality consisted mostly of diatom frustules, clay minerals, and organic matrices. As was the case with the C_1 site, zinc was predominantly associated with iron-phosphorus rich particles. In addition to these particles, zinc was also found present at significant concentrations on iron-manganese rich precipitates on bacterial cell walls (Figures 6.1c and 6.2c). Again, these observations demonstrate the intimate relationships between biological structures (*i.e.* cell walls) and zinc partitioning. Additionally, these TEM observations suggest that biological surfaces are acting as

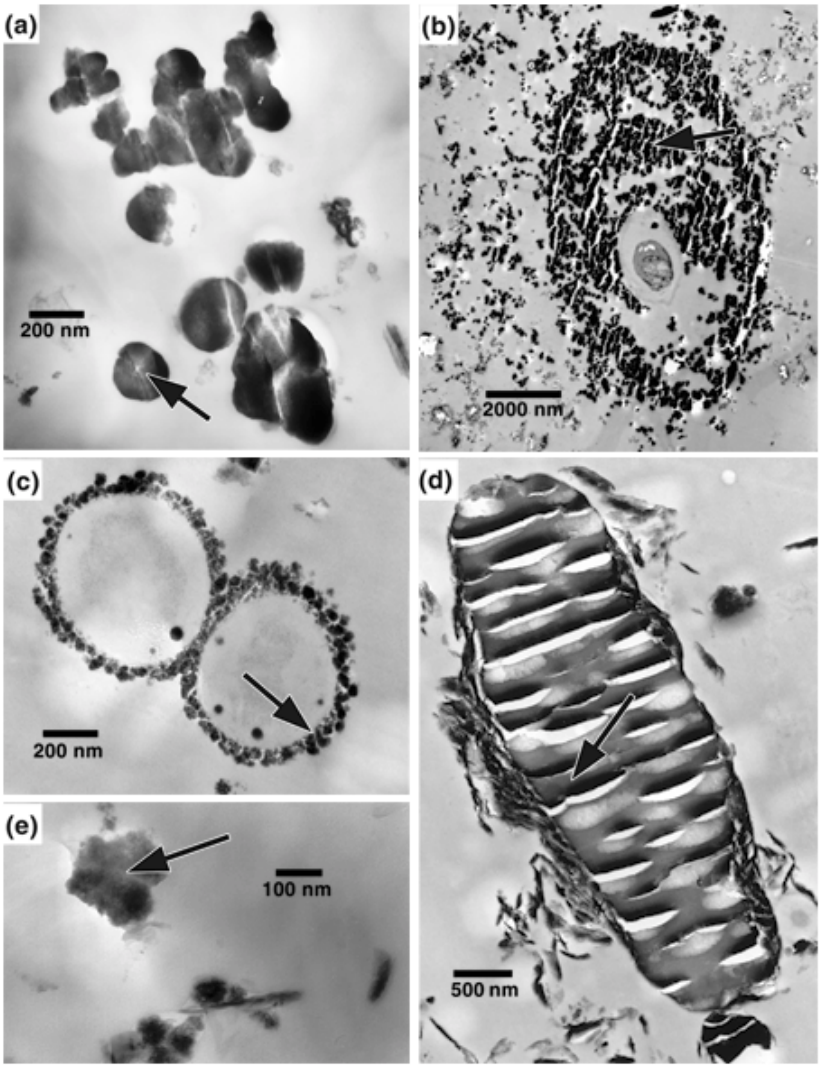

Figure 6.1: TEM micrographs of particles imaged from Lake DePue. The images shown are representative of key features in the lake, and are a subset of over 250 observations. The arrow in each picture shows where the EDS spectrum was collected (see Figure 6.2). **(a)** Well crystalline, regular shaped globules found in the creek sediments (C_1) of Lake DePue. The particles are noted to have a uniform electron density and have very well defined edges. The globules are the dominant morphology of zinc containing particles in this region. **(b)** Algal cell (center) surrounded by a large number of zinc containing particles at site C_1. Biological membranes in this micrograph were enhanced with a uranyl acetate stain. **(c)** Bacterial cells in the water column collected at site C_2. The electron density of the precipitate at the bacterial wall is due to the presence metals. Bacteria and other similar biological structures are the principal morphology of zinc containing particles in the water column of the lake. **(d)** Diatom frustule found in the water column of Lake DePue at C_2. **(e)** Globules collected from sediments at the creek outlet (C_2) which show irregular electron density, suggesting an amorphous nature. (Webb, *et. al.*, 2000)

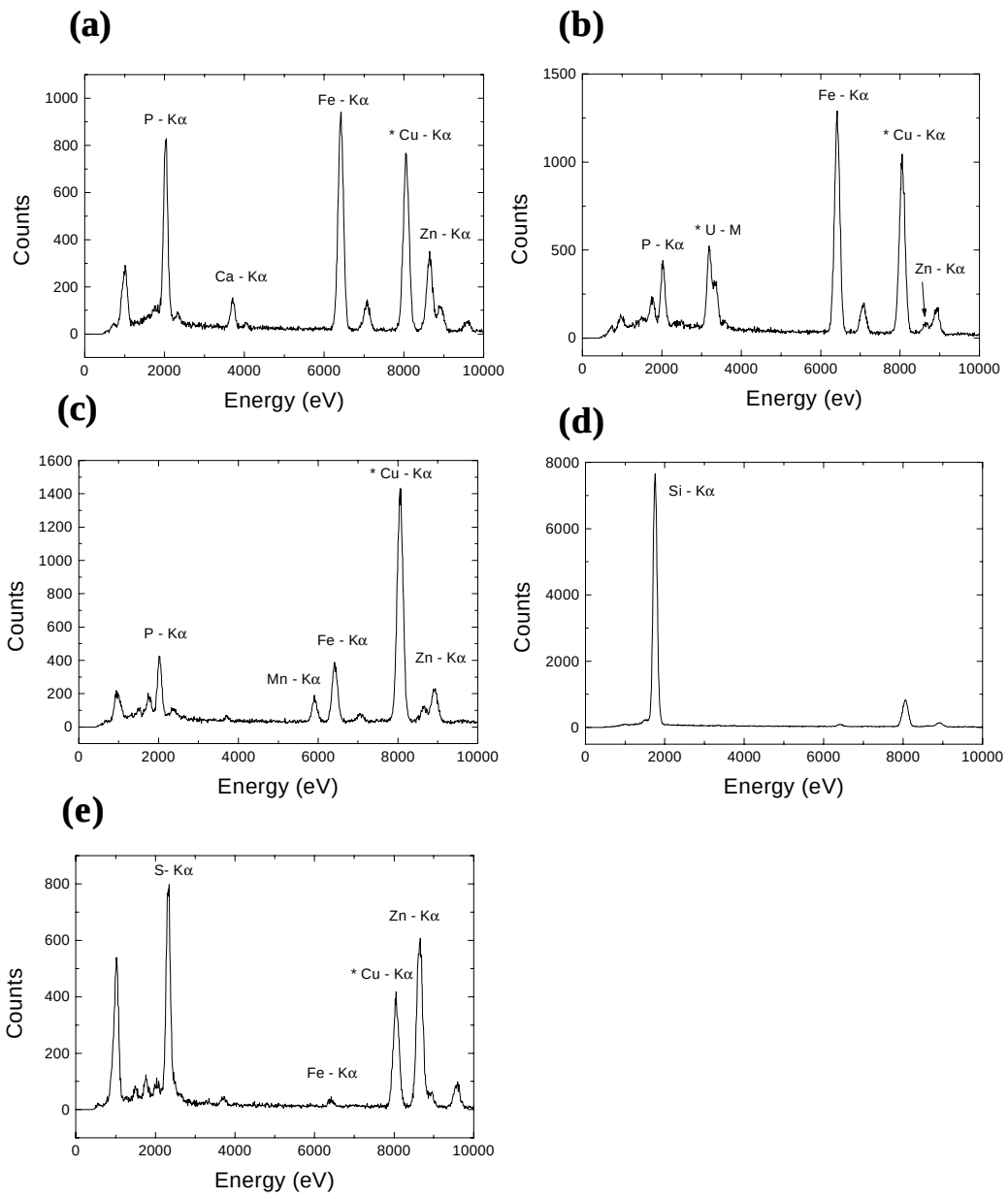

Figure 6.2: EDS spectra collected from the particles shown in Figure 6.1. Peaks labeled with an asterisk are contaminant peaks. **(a)** Well crystalline globules from C_1 are composed primarily of Fe-Zn-phosphates. These particle associations are ubiquitous throughout the C_1 sediments and C_2 water column. The contaminant peak from Cu is due to the Cu grid. **(b)** Particles entrained in algal associations are again composed primarily of Fe-Zn-phosphates. The U peak in the spectrum is from the uranyl acetate stain used to enhance organic membranes. **(c)** Cell wall precipitates found on bacterial cells are composed mostly of Fe and Mn. Zn is also found in association with these precipitates and has likely been scavenged from the water column. **(d)** In contrast to the biological precipitates found on microbial cell walls, diatoms, which are found in large numbers throughout the lake, do not have any Zn present in their structures within the detection limits of the EDS. **(e)** Amorphous particles in the anaerobic sediments show a strong association of Zn and S. This is suggestive of a diagenetic formation of ZnS at depth in the sediments. The EDS spectrum shows that the particles are relatively pure, containing very little iron or other metals. (Webb, *et. al.*, 2000)

templates for the formation of zinc-rich particles. Zinc was rarely detected on any of the clay minerals present in the water column of the lake, and was never measured above detection limits in diatom frustules or biogenic silica particles represented by frustule fragments (Figures 6.1d and 6.2d).

Figures 6.1e and 6.2e show the micrograph and EDS spectrum of sediment collected in the lake at the outlet of the effluent creek (C_2). The sediments in the lake become anaerobic very rapidly, in contrast to the more oxic sediments at C_1. The zinc contamination in this region of the lake is still significant, but much smaller than at C_1. Sediment zinc concentrations range from 1% to 5% by dry weight. Particles containing measurable concentrations of zinc in C_2 sediments fall into a much narrower type classification than at C_1. The most common particulate form of zinc is shown in Figure 6.1e. These are small, rounded globules, typically 45-210 nm (average 82 nm) in diameter, that appear to consistently have poorly defined edges and extremely irregular electron density, suggestive of an amorphous nature. The zinc in these particles is nearly always present with a large concentration of sulfur. The sulfur in anoxic sediments associated with zinc is most likely to be in the form of sulfides. This suggests that there is diagenetic formation of ZnS in the sediments at this location. In addition to these globules, zinc is also present in a significant fraction in mineralized layers. EDS spectra from these mineralized materials show also strong zinc and sulfur contributions.

Sediments were also collected from a mid-lake site (M_1), which has a much lower level of zinc contamination. Typical zinc concentrations at this location range from a

background level of 50 ppm to 0.5% by dry weight. Consequently, zinc is found to be abundant in relatively few particles as detected by EDS. Particles in this region consisted mostly of biogenic silica, clay minerals, and bacterial cells. At this site, zinc was primarily found to be associated with sulfur.

6.2 QUANTITATIVE RESULTS

The average elemental composition of each of the major particle classifications for each sampling location is presented in Table 6.1. Note that these are the percent compositions, on a mole basis, of the elements measured within the analytical window of the EDS detector. Since a Be window was used, these compositions do not include the concentration of lighter elements such as C, N, and O. Several conclusions emerge from these data. First, the major element composition (*i.e.*, Si, Al, Mg, K) of the clay particle classification remains nearly the same at all three sampling locations. This is not surprising, since the clay particles are likely derived from the same Quaternary glacial sedimentary sources in the region. Second, based on the overall average elemental composition for the clay mineral morphology, the clays consist of a mixture of illite, chlorite, and kaolinite (Klein and Hurlbut Jr., 1993), and zinc concentrations present on these particles decrease from C_1 to C_2 to M_1 as expected by the drop in the contaminant levels between these sites. The presence of zinc in this carrier phase is likely due to sorption processes either onto clay minerals or onto iron oxide coatings precipitated on the clays. We can also notice here that there is no obvious correlation between Zn and Fe concentrations in this clay particle category. Last, a similar trend in zinc concentration is

Table 6.1: The average elemental compositions of the major particle morphologies. The table shows the composite average of all particles of a given morphology over all of the collection sites, as well as the breakdowns of the composition at each individual site. Oxides and Clay mineral have been grouped together. (Webb, *et. al.*, 2000)

average-C_1	Morphology	Zn	Fe	P	S	Si	Al	Na	Mg	K	Ca	Mn	Ti	Pb	Ba	Ni
	Oxide Clay	1.42	2.80	4.89	0.37	57.55	23.18	0.00	6.67	2.20	0.88	0.00	0.05	0.00	0.00	0.00
	Globule	5.66	15.45	53.62	1.83	10.14	7.46	1.54	2.79	0.00	1.51	0.00	0.00	0.00	0.00	0.00
	Sulfide	0.00	0.00	0.00	0.00	0.00	0.00	0.00	0.00	0.00	0.00	0.00	0.00	0.00	0.00	0.00
	Organic	2.21	7.90	23.79	20.62	29.57	12.26	0.00	3.31	0.00	0.32	0.00	0.00	0.00	0.00	0.00
	Diatom	0.16	0.20	0.00	0.00	98.34	1.29	0.00	0.00	0.00	0.00	0.00	0.00	0.00	0.00	0.00
	Carbonate	0.00	0.00	0.00	0.00	0.00	0.00	0.00	0.00	0.00	0.00	0.00	0.00	0.00	0.00	0.00

average-C_{2s}	Morphology	Zn	Fe	P	S	Si	Al	Na	Mg	K	Ca	Mn	Ti	Pb	Ba	Ni
	Oxide Clay	1.39	4.65	1.83	1.46	55.39	25.16	0.00	6.08	3.42	0.50	0.03	0.10	0.00	0.00	0.00
	Globule	0.00	0.00	0.00	0.00	0.00	0.00	0.00	0.00	0.00	0.00	0.00	0.00	0.00	0.00	0.00
	Sulfide	13.54	0.64	2.89	55.23	15.28	7.63	0.00	2.82	0.15	0.50	0.00	0.00	0.00	1.31	0.00
	Organic	2.33	7.24	2.45	4.25	55.94	21.55	0.00	5.11	0.50	0.52	0.00	0.11	0.00	0.00	0.00
	Diatom	0.00	0.13	0.00	0.35	98.57	0.95	0.00	0.00	0.00	0.00	0.00	0.00	0.00	0.00	0.00
	Carbonate	0.21	1.60	12.27	0.68	14.00	8.52	0.00	38.34	0.34	23.95	0.10	0.00	0.00	0.00	0.00

average-C_{2w}	Morphology	Zn	Fe	P	S	Si	Al	Na	Mg	K	Ca	Mn	Ti	Pb	Ba	Ni
	Oxide Clay	0.41	3.72	3.73	1.34	52.61	30.31	0.00	4.49	2.92	0.17	0.00	0.12	0.19	0.00	0.00
	Globule	2.06	7.32	53.72	4.09	16.34	14.73	0.00	0.63	0.04	1.07	0.00	0.00	0.00	0.00	0.00
	Sulfide	0.00	0.00	0.00	0.00	0.00	0.00	0.00	0.00	0.00	0.00	0.00	0.00	0.00	0.00	0.00
	Organic	1.83	7.33	43.90	5.16	24.45	14.48	0.00	0.00	0.06	0.85	1.94	0.00	0.00	0.00	0.00
	Diatom	0.06	0.19	0.50	0.00	94.57	3.94	0.00	0.00	0.30	0.13	0.05	0.27	0.00	0.00	0.00
	Carbonate	0.04	0.42	0.41	0.33	12.18	4.44	0.00	62.35	0.07	19.73	0.04	0.00	0.00	0.00	0.00

average-M_1	Morphology	Zn	Fe	P	S	Si	Al	Na	Mg	K	Ca	Mn	Ti	Pb	Ba	Ni
	Oxide Clay	0.16	5.13	2.74	3.20	48.06	29.45	0.00	5.71	3.12	0.17	0.00	0.09	2.03	0.00	0.13
	Globule	0.00	0.00	0.00	0.00	0.00	0.00	0.00	0.00	0.00	0.00	0.00	0.00	0.00	0.00	0.00
	Sulfide	14.17	3.87	1.05	39.65	16.42	14.86	0.00	2.25	0.00	0.80	0.00	0.00	6.93	0.00	0.00
	Organic	0.83	9.15	2.12	18.24	25.76	27.54	0.00	1.09	0.77	2.14	0.00	0.00	12.32	0.00	0.03
	Diatom	0.03	1.32	0.38	0.00	86.29	9.45	0.00	0.81	1.16	0.54	0.00	0.00	0.02	0.00	0.00
	Carbonate	0.01	0.66	0.00	0.44	23.83	9.48	0.00	15.75	0.28	49.28	0.00	0.16	0.00	0.00	0.11

also seen in the organic material. In this context, the organic material consists of bacterial cells, microalgae, capsular layers, and fibrils. Again, the zinc present in this material is due certainly to the presence of specific metal binding sites, and the amount of zinc decreases as the level of contamination decreases.

Analytical EDS provides estimates of the elemental ratios of the major zinc bearing phases found in Lake DePue. The analyses of the globules rich in Fe, P, and Zn found in the C_1 sediments show that the amount of phosphorus present remains relatively constant. In these particles, P accounts for 63% ± 5% of the elements measured within each spectrum (this composition does not include light elements such as C, N, and O). In contrast, the distribution of iron and zinc in these particles is much more variable, although the sum of the relative concentrations of these two elements is quite constant, typically 24% ± 4%. The concentrations of iron and zinc, however, are anti-correlated. A plot of Fe vs. Zn (Figure 6.3) shows a slope of -1.08 ± 0.12 with a correlation coefficient of 0.704. This suggests that zinc and iron are substituting for each other within the matrix of these particles. Although the anti-correlation holds for the collection of different particles taken from the same location, the elemental proportions of Zn and Fe in an individual particle are closely related, as shown in the EDS cross-section shown in Figure 6.4. In the cross-section of this relatively low Zn particle, the proportions of Zn and Fe appear well correlated and rather uniform across the diameter of the particle. The observation that individual particles are uniform in their iron-zinc ratios, whereas the ensemble of particles shown an inverse correlation suggests that these particles may have formed authigenically in the sediment along the gradient of contamination. In this

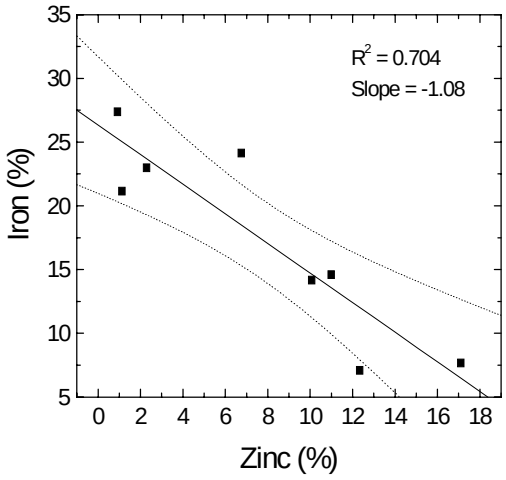

Figure 6.23: Anti-correlation plot of iron vs. zinc in phosphate rich globules with the 95% confidence interval shown in the dashed lines.

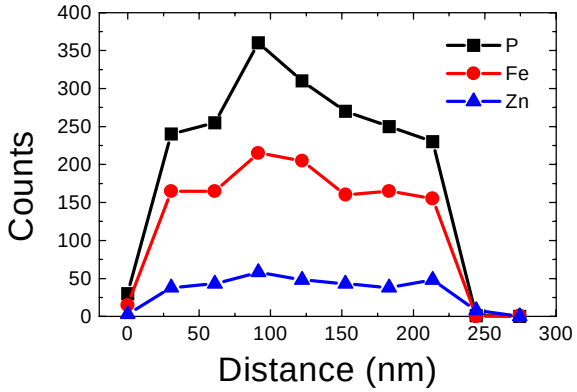

Figure 6.4: Integrated EDS peak area of elements P, Fe, and Zn across particles similar to that in Figure 6.1a and Figure 6.3. Total particle diameter was approximately 220 nm. Relative proportions of elements are approximately constant across the particle.

manner, individual particles will have differing iron-zinc ratios depending on the local concentration of zinc where the particle was formed, while the total metal cation to phosphate ratio remains the same in all particles. The uniformity of the iron and zinc across the particle supports this hypothesis over a zinc-adsorption or zinc-uptake mechanism for the formation of the particles.

Globules in the water column of C_2 are slightly different in nature. They show a more consistent concentration of Fe, and they contain proportionally more phosphate (P: 57% ± 5.3%, Fe 7.0% ± 0.8%; Zn 2.2% ± 0.8 %). At this location, cation substitution between iron and zinc does not appear to be as important as in C_1, since the relative concentration of iron remains nearly constant whereas the fraction of zinc varies. Similar observations can be made for the zinc and sulfur rich particles in the sediments at C_2 and M_1. Since the particles were sampled from the anaerobic zone of the sediments, the dominant form of sulfur bound with zinc or iron is likely to be sulfide. The average elemental ratios measured at these two sites were Zn:S = 1:4 at C_2, and Zn:Fe:S = 1.2:0.3:3 at M_1, with Zn composing approximately 14% ± 3% of the relative particle composition.

Figure 6.5 shows the cluster diagrams of the major elements determined by STEM-EDS. These relations were calculated using the relative concentrations of each element, as determined by standardless ZAF analysis (Fiore *et. al.*, ; Reed, 1993) of the EDS measurements. The cluster diagram approach consists of a hierarchical grouping of variables, based the similarity of their behavior. Thus, we can determine which chemical elements are closely related to each other at each sampling location. Significant changes in zinc-bearing phases between the sampling sites can be seen in these diagrams. In the creek sediments (C_1) zinc is associated most strongly with iron, phosphorus, and calcium. The association with calcium occurs as a result of a calcium phosphate rich (apatite) particle that was examined from this site, which skewed the calcium-phosphorus relationship. These elements are in a distinct group from the elements that

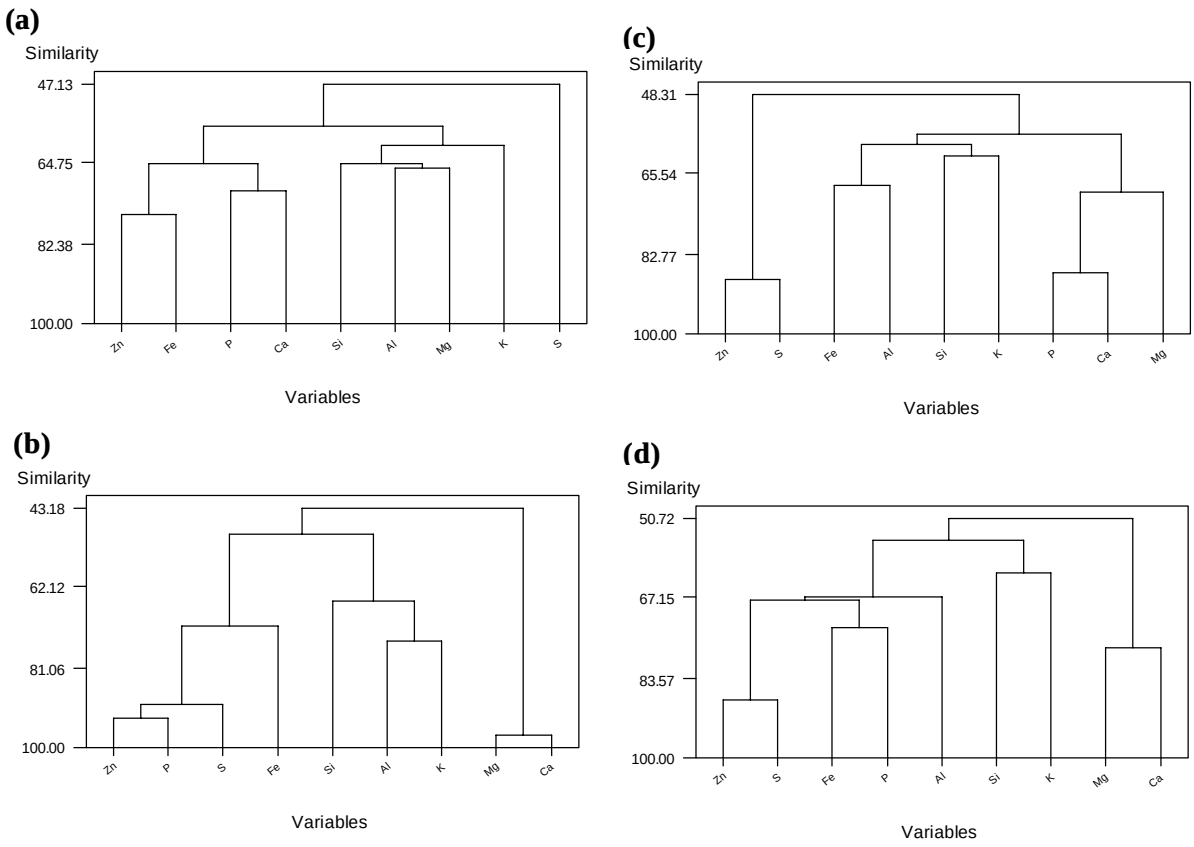

Figure 6.5: Cluster diagrams based on the ZAF corrected concentrations of each element for each of the sampling locations. The pattern of the elemental associations of zinc can be seen in these figures, from mainly zinc-iron-phosphate relationships to zinc-sulfur relationships. **(a)** C_1 sediment cluster diagram, which is a composite of 50 observations. **(b)** C_2 water column cluster diagram, a composite of 42 observations. **(c)** C_2 sediment cluster diagram, a composite of 34 observations **(d)** M_1 sediment cluster diagram, a composite of 28 observations. (Webb, *et. al.*, 2000)

compose most of the clay minerals (Si, Al, Mg, and K). In the water column of the lake, however, zinc is associated primarily with phosphorus and sulfur, and to a lesser degree with iron. Again, this grouping is distinct from the clay mineral group (Si, Al, and K) and the carbonate group (Mg and Ca). The sediments in the lake (C_2 and M_1) are again

significantly different from the other sampling sites. The cluster analysis shows that, at these sampling locations, zinc is associated almost exclusively with sulfur.

The iron-zinc-phosphorus particles from C_1 may have several possible origins. First, they may have originated from the industrial smelting processes, and may have been transported to the lake through groundwater and surface water runoff. Second, as the concentrations of iron and zinc are relatively high in the surface waters of C_1, the particles could have formed through an abiotic, *in situ* precipitation. Last, these particles could have resulted from a biological process, either intracellular or extracellular, that leads to the precipitation of phosphate compounds. This last hypothesis seems to be likely since the particles appear to be intimately associated with biological cells (Figure 6.1b) and, in many cases, are surrounded by extracellular structures. Other biotic structures, such as intracellular polyphosphates and iron-phosphorus rich granules, have been observed directly by TEM and STEM-EDS (Bode *et. al.*, 1993; Lins and Farina, 1999) for bacteria. Metal-phosphate granules have also been observed in the phosphate metabolizing bacteria *Acinetobacter johnsonii* when grown in pure culture along with cadmium (Boswell *et. al.*, 1999). In any case, our TEM observations exemplify that the distribution of zinc is inherently related to biological structures at nearly every sampling location probed. These structures are not only the dominant carriers of zinc in the lake, but may also act as an important catalyst site for the formation of these particles. More work is necessary to understand the actual processes that are occurring at the level of cell walls, and that are leading to the formation of the colloidal particles observed. Some pertinent results have been reported in the literature, and provide some guidelines for

our further studies. The fibrils (extracellular polymeric substances), which extend from the surfaces of some bacteria, possess nucleation sites for the deposition of iron and manganese oxides (Ghiorse and Hirsch, 1979). Bacterial cell walls can remove metals from dilute solutions, including simulated lake water (Mayers and Beveridge, 1989), and bacterial metal accumulation has been well documented in regard to cell wall interactions with metals in solution (Beveridge and Doyle, 1989; Schultze-Lam *et. al.*, 1996). The generation of mineralized (Ca, Si) scales and wall parts of colloidal dimensions, by internal metabolic processes in microalgae, is a phenomenon well documented, including its ultrastructural aspects (Dodge, 1973). Colloidal iron associations with surfaces of many kinds are currently being documented for suspended native particles in (iron / phosphate / organic carbon-rich) lake water (Pizarro *et. al.*, 1995). With regard to mineral coatings on bacteria, studied *in situ* in native sediments, it has been shown recently by STEM-EDS that iron oxyhydroxide coatings on cell walls and extracellular fibrils will strongly and preferentially accumulate copper from pore water (Jackson *et. al.*, 1999). These works, and the present one, stress the importance of examining the micro-scale to elucidate important contaminant bearing phases present in aquatic ecosystems; they also stress the importance of considering biological templates as an important factor in contaminant transformations.

However, there exist some limitations inherent to this method of particle analysis. First, X-ray EDS provides only elemental concentrations. It is impossible to differentiate sulfide from sulfate for example, and some biogeochemical intuition is. Second, the EDS detector is only sensitive to relatively high elemental concentrations (greater than 0.1%).

Thus, classes of particles that contained a small concentration of zinc, but that may be numerous enough to make up a significant fraction of the total particulate metal concentration, would be missed by this technique. This problem can be remedied by using complementary analytical techniques. In particular, a spectroscopic technique, such as XAS (X-ray absorption spectroscopy), can be used to probe the average local coordination environment of metals (Lamoureux *et. al.*, 1995; Manceau *et. al.*, 1996), and actually it proves to be quite advantageous in this case since zinc is known to be spectroscopically silent by other methods. These investigations will be reported in the next section.